Journal of Applied Physics

RESEARCH ARTICLE | OCTOBER 16 2024

Attainment of high critical current in thick $BaZrO_3$-doped $YBa_2Cu_3O_7$ multilayer nanocomposite films

Victor Ogunjimi ; Mohan Panth ; Mary Ann Sebastian ; Jianan Shen ; Matteo Moceri ; Charles Ebbing; Timothy Haugan ; Haiyan Wang ; Aafiya ; Judy Wu

J. Appl. Phys. 136, 155302 (2024)
https://doi.org/10.1063/5.0231956

Journal of Applied Physics ARTICLE pubs.aip.org/aip/jap

Attainment of high critical current in thick $BaZrO_3$-doped $YBa_2Cu_3O_7$ multilayer nanocomposite films

Cite as: J. Appl. Phys. **136**, 155302 (2024); doi: 10.1063/5.0231956
Submitted: 3 August 2024 · Accepted: 1 October 2024 ·
Published Online: 16 October 2024

Victor Ogunjimi,[1] Mohan Panth,[1] Mary Ann Sebastian,[2,3] Jianan Shen,[4] Matteo Moceri,[4] Charles Ebbing,[2] Timothy Haugan,[2] Haiyan Wang,[4] Aafiya,[1] and Judy Wu[1,a)]

AFFILIATIONS

[1]Department of Physics and Astronomy, The University of Kansas, Lawrence, Kansas 66045, USA
[2]U.S. Air Force Research Laboratory, Aerospace Systems Directorate, Wright-Patterson AFB, Ohio 45433, USA
[3]University of Dayton Research Institute, Dayton, Ohio 45469, USA
[4]School of Materials Engineering, Purdue University, West Lafayette, Indiana 47907, USA

[a)]**Author to whom correspondence should be addressed:** jwu@ku.edu

ABSTRACT

High critical current (I_c) in high magnetic fields (B) with minimal variations with respect to the orientation of the B field is demanded by many applications such as high-field magnets for fusion systems. Motivated by this, this work studies 6 vol. % $BaZrO_3/YBa_2Cu_3O_7$ (BZO/YBCO) multilayer nanocomposite films by stacking two 10 nm thick $Ca_{0.3}Y_{0.7}Ba_2Cu_3O_7$ (CaY-123) spacers with three BZO/YBCO layers of thickness varied from 50 to 330 nm to make the total film thickness of 150–1000 nm. The Ca diffusion from the spacers into BZO/YBCO was shown to dramatically enhance pinning efficiency of c-axis aligned BZO nanorods, which yields high and almost thickness independent critical current density (J_c) in the BZO/YBCO multilayer nanocomposite films. Remarkably, enhanced J_c was observed in these multilayer samples at a wide temperature range of 20–80 K and magnetic fields up to 9.0 T. In particular, the thicker BZO/YBCO multilayer films outperform their thinner counterparts in both higher value and less anisotropy of J_c at lower temperatures and higher fields. At 20 K and 9.0 T, I_c is up to 654 A/cm-width at B//c in the 6% multilayer (1000 nm) sample, which is close to 753 A/cm-width at B//ab due to the intrinsic pinning. This result illustrates the critical role of the Ca cation diffusion into the YBCO lattice in achieving high and isotropic pinning in thick BZO/YBCO multilayer films.

I. INTRODUCTION

High-temperature superconducting (HTS) materials have the potential in a variety of electric power applications, such as transmission cables, motors, and high-field magnets for large accelerators and fusion systems as they can carry a large amount of current in high magnetic fields (B).[1–4] One of the most widely used HTS materials is $YBa_2Cu_3O_{7-x}$ (YBCO), which has been used extensively in coated conductors and has demonstrated a high critical current density (J_c).[1,5–9] For practical applications, increasing the thickness of YBCO to a few micrometers can improve critical current (I_c) and reduce manufacturing costs that will ultimately impact the marketability of second-generation coated conductors.[10] It is, therefore, important to achieve high J_c in thick YBCO films at high magnetic fields[11–13] through self-assembly of various types of vortex-pinning centers, known as artificial pinning centers (APCs).[14–16] Among others, one-dimensional APCs (1D-APCs) aligned along the c-axis of YBCO have been studied intensively since they can provide correlated pinning at the B//c-axis addressing the weak pinning associated to the layered structure of $REBaCu_3O_{7-x}$ (RE regards rare earth elements of Y, Gd, and Sm). Examples include $BaZrO_3$ (BZO), $BaSnO_3$ (BSO), $BaHfO_3$ (BHO), and $YBa_2(Nb/Ta)O_6$ 1D-APCs that have been grown in $REBaCu_3O_{7-x}$ (RE regards rare earth elements of Y, Gd, and Sm) films to provide strong correlated pinning at the B//c-axis.[15,17–25]

In a recent study, we have found the pinning efficiency of BZO 1D-APCs can be enhanced substantially by diffusing a small number of Ca ions into the YBCO lattice in the BZO/YBCO nanocomposite thin films using a multilayer (ML) approach.[26] Specifically, Ca is provided from two thin spacers of $Ca_{0.3}Y_{0.7}Ba_2Cu_3O_7$ (CaY-123) with 5–15 nm in thickness grown alternatively with three BZO/YBCO layers each of ∼50 nm in the thickness in the ML samples. Ca/Cu replacement on the Cu–O planes of the YBCO lattice near the BZO 1D-APC/YBCO interface was observed in a microstructure study using high-resolution scanning transmission electron microscopy.[27] The short segments of stacking faults formed at the Ca/Cu–O planes leads to the c-axis elongation of YBCO near the BZO 1D-APC/YBCO interface, resulting in reduced lattice mismatch from ∼7.7% to 1.4% and hence an almost defect-free interface.[27–30] While a J_c enhancement by up to 440% was achieved on ∼150 nm thick BZO/YBCO ML films at 65 K and 9.0 T, it remains a question on whether sufficient Ca diffusion efficacy could be achieved in the same five-layer structured ML films when the film thickness ≫150 nm. In order to answer this question, this work presents an investigation of 6 vol. % BZO/YBCO ML samples as the constituent BZO/YBCO layer thickness is varied from 50 to 330 nm or the total film thickness varied from 150 to ∼1000 nm with the same two CaY-123 spacers of a fixed thickness of 10 nm each. Remarkably, comparable J_c was observed in these films in a wide temperature range of 20–80 K and field range of 0–9.0 T. Interestingly, thicker ML films outperform their thinner counterparts in both J_c values and reduced J_c anisotropy at lower temperatures and higher fields. These findings suggest that Ca diffusion facilitated by the tensile strained BZO 1D-APC/YBCO interface could be highly efficient in the BZO/YBCO ML samples of large thicknesses with enhanced pinning for high J_c values in a wide temperature range at high magnetic fields.

II. METHODS

A. Fabrication of multilayer BZO/YBCO nanocomposite films

BZO/YBCO nanocomposite ML films with BZO concentration of 6 vol. % were fabricated using pulsed laser deposition (PLD) from a BZO-doped YBCO target of the same nominal compositions. Single-crystalline (100) oriented on $SrTiO_3$ (STO) substrates were used. For the purpose of comparison, the same BZO-doped YBCO target was also used to make BZO/YBCO single-layer (SL) films of selected thicknesses using the same PLD condition, especially the same 8 Hz repetition rate. This means the ML and SL samples would be otherwise the same except the former contains two CaY-123 spacers of 10 nm each in thickness. In order to make ML samples, a CaY-123 PLD target was adopted for PLD deposition (at repetition rate of 2 Hz) of the two CaY-123 spacer layers of thickness ∼10 nm each alternatively with BZO/YBCO layers. The five-layer ML samples consist of three BZO/YBCO layers as the 1st, 3rd, and 5th layer and two CaY-123 spacers as the 2nd and 4th layer. Since the starting layer (or 1st layer) in the ML sample is also BZO/YBCO, the same nucleation of BZO 1D-APCs on the STO substrate is anticipated in the 1st BZO/YBCO layer of the ML samples to that in the counterpart SL ones. While the BZO 1D-APCs cannot grow through the thin CaY-123 spacers, they have been found to continue in the BZO/YBCO layer on top of thin CaY-123 spacers,[26] yielding comparable areal density and diameter of the BZO 1D-APCs in ML and SL samples at the same BZO doping. All samples were annealed *in situ* at 500 °C in one atmospheric oxygen pressure for 30 min after the PLD deposition. More details of the ML film growth were described in previous studies.[26–29] The film thicknesses were measured using a Tencor P-16 profilometer. The ML films have nominal thicknesses of 150, 300, 450, 600, 750, and 1000 nm, respectively, which were confirmed using a Thermo Fisher Scientific Tencor P16 3D surface profiler to be within a few percents. The measured film thicknesses were used for the calculation of J_c. For convenience, these ML samples are regarded as 6% ML (150 nm), 6% ML (300 nm), 6% ML (450 nm), 6% ML (750 nm), and 6% ML (1000 nm) samples, respectively, in the discussion below.

B. Characterization of multilayer BZO/YBCO nanocomposite films

Scanning transmission electron microscopy (STEM) was adopted to study the microstructures of the samples using a Thermo Fisher Scientific Themis-Z TEM system which is an aberration-corrected electron microscope with a spatial resolution as small as 63 pm at an acceleration voltage of 300 kV with combined correctors. Energy dispersive x-ray spectroscopy (EDS) was used to analyze the element distribution across the ML cross-sectional area. Crystallinity and lattice parameters were determined by x-ray diffraction (XRD) utilizing a Bruker D8 Discover diffractometer.

For electrical transport measurements, two parallel microbridges were fabricated on each film using standard photolithography using the same protocol reported in our previous works.[31,32] Wet etching in 0.05% of nitrous acid was adopted to complete the fabrication of the two microbridges of bridge length of 500 μm and bridge width of 20 and 40 μm, respectively. To make the electric contact, Ag contact pads of ∼1 mm in diameter and ∼120 nm in thickness were deposited through a shadow mask using DC magnetron sputtering before photolithography to prevent sample surface contamination by chemicals and solvents used for lithography. The electric power used for the Ag sputtering is 34 W, which yielded a deposition rate of approximately 0.07 nm/s under the argon pressure of 30 mTorr. The electrical connection to the microbridges were completed by attaching platinum wires of 50 μm in diameter on the Ag pads using indium. J_c was measured at different applied magnetic fields B in the range of 0–9.0 T at temperatures in the range of 20–80 K in a Quantum Design Ever-Cool II Physical Property Measurement System (PPMS). The standard four-probe technique was used while measuring the transport properties (T_c and J_c). Current–voltage (I–V) curves was taken using a HP 34420A nanovoltmeter and a Keithley 2430 1 KW Pulse Source Meter at different B field orientations ranging from $\theta = 0°$ (B//c-axis) to $\theta = 90°$ (B//ab-plane) in the plane with B perpendicular to J_c. The J_c values were determined by applying a standard voltage criterion of 1 μV/cm on the I–V curves. The pinning force density (F_p) was evaluated by using the equation $\boldsymbol{F_p = J_c \times B}$. The maximum pinning force density ($F_{p,max}$) and its corresponding location of the magnetic field (B_{max}) were then determined from the F_p (B) curves.

III. RESULTS AND DISCUSSION

Figure 1 illustrates schematically the cross-sectional microstructures of BZO/YBCO SL and ML films with the same BZO doping level. The SL film contains an array of c-axis aligned BZO 1D-APCs (black) grown throughout the entire film thickness of the YBCO film [Fig. 1(a)]. The ML sample [Figs. 1(b) and 1(c)] has a five-layer structure with two 10 nm thick CaY-123 spacers grown alternatively with three BZO/YBCO layers each having thickness varied in the range of 50–330 nm. This leads to the total film thickness varied in the range of about 150–1000 nm. Since these ML samples have the same CaY-123 spacers, the total amount of Ca is maintained the same. However, since the same PLD growth conditions, especially the same PLD repetition rate of 8 Hz for BZO/YBCO layers, were applied to grow BZO/YBCO ML films of different thickness, the diffusion time for Ca ions would increase linearly with the BZO/YBCO layer thickness due to a longer growth time required for PLD deposition at the same repetition rate. The purpose of restricting the Ca amount is to minimize reduction of Ca/Y replacement on YBCO lattice which leads to reduced critical temperature T_c due to the consequent overdoping effect on YBCO.[33–35] This argument is based on strain-mediated Ca substitutions of Y, Ba, and Cu from density function theory simulation.[36] Near the BZO 1D-APC/YBCO interface, the higher tensile strain would make Ca diffusion and Ca/Cu replacement more favorable energetically since Ca ion is about 30% larger in size than Cu ion. If this hypothesis prevails, Ca diffusion along the BZO 1D-APC/YBCO interface could proceed at a large thickness of the BZO/YBCO layer considering only a small amount of Ca is needed for the Ca/Cu replacement in the C–O plane to enlarge the c-axis of YBCO near the BZO 1D-APC/YBCO interface and no more Ca would be needed when the c-axis elongation is adequate.

Figures 2(a) and 2(b) exhibit STEM cross-sectional views of 6% BZO/YBCO ML samples of 150 and 600 nm total thicknesses, respectively. The five-layer structure consisting of two CaY-123 spacers and three BZO/YBCO layers can be clearly seen in both cases. Through the film thickness, each BZO 1D-APC has three segments due to the presence of the two CaY-123 spacers. The segments align well on top of each other through the entire film thickness in both 150 and 600 nm thick ML samples. This means that the presence of the thin spacers does not seem to perturb the modulated strain field formed in the BZO/YBCO layers, which is driving force in nucleation and evolution of the c-axis aligned BZO 1D-APCs. Furthermore, since the first layer of the ML samples is BZO/YBCO fabricated in the same way as in the BZO/YBCO SL samples, the nucleation of the BZO 1D-APCs is expected to be the same in the SL and ML samples. This means the same morphology, dimension and concentration of BZO 1D-APCs are expected in SL and ML samples under the same BZO doping. This argument is supported by the quantitative analysis of TEM data. For example, the diameter of the BZO 1D-APCs in the ML samples is around 5–6 nm and the center-to-center spacing (d) between BZO 1D-APCs is around 12 nm for the 6% ML (600 nm) sample [Fig. 2(c)]. The BZO 1D-APC linear density is hence ~83/μm, which is comparable to that for their SL counterpart and that in the 6% ML (150 nm) sample.[23,27] The BZO 1D-APC concentration allows the estimation of the accommodation field defined as $B^* = \Phi_o/d^2 \sim 14.3$ T, where $\Phi_o = 2.07 \times 10^{-15}$ Wb is the flux quantum. Figures 2(d)–2(f) show the EDS maps of Ca, Zr, and Y on the 6% ML (150 nm) sample in Fig. 2(a), the elemental distributions agree well with the expectation. In particular, the amount of Ca remaining in the two spacers is fairly high, which suggests the amount of Ca ions diffused into the BZO/YBCO layers is most probably limited. This is not surprising as no obvious defective, and hence efficient, diffusion channels are present in the ML samples. In the case of YBCO films on bicrystals, grain boundaries are highly defective and are found to serve as highly efficient

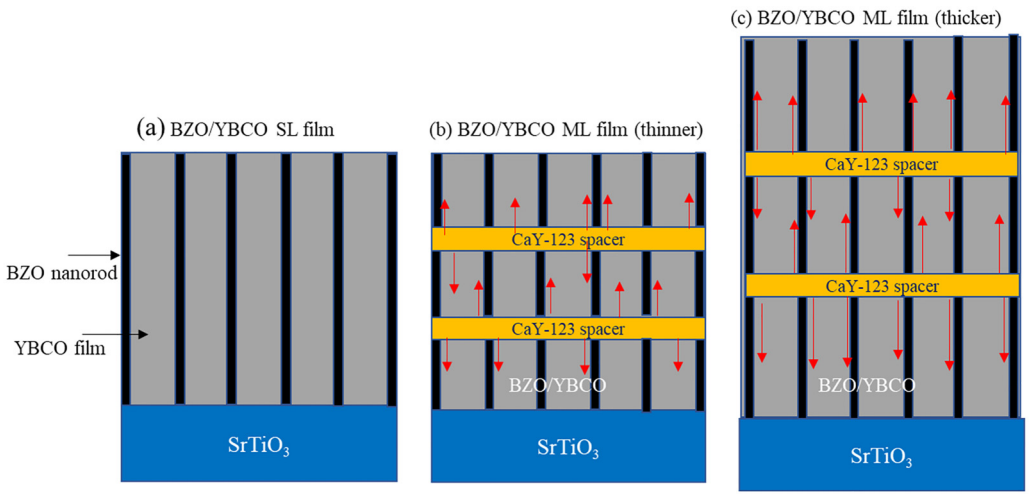

FIG. 1. Schematic diagrams of (a) BZO/YBCO film SL and BZO/YBCO ML films with two 10 nm thick CaY-123 spacers and three thinner (b) or thicker (c) BZO/YBCO layers each having thickness in the range of 50–330 nm.

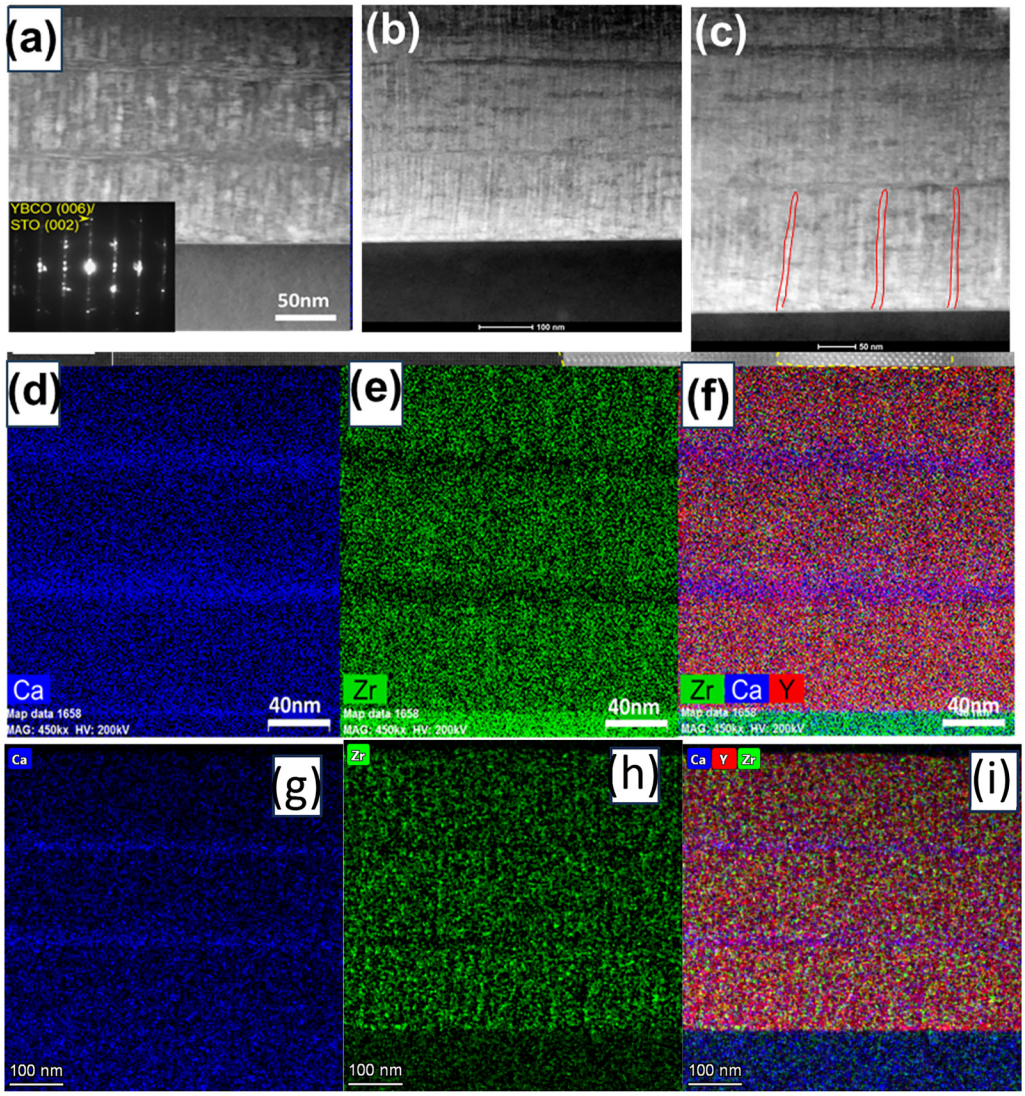

FIG. 2. Cross-sectional STEM images of the 6% BZO/YBCO ML films of (a) 150 and (b) 600 nm thicknesses, respectively. (c) Zoom-in view of (b) for a quantitative analysis of BZO 1D-APC concentration of ~83/μm. EDS mappings of Ca, Zr, and combined Ca, Y, and Zr are shown in (d)–(f) for the 150 nm and (g)–(i) for the 600 nm thick ML samples.

diffusion channels for Ca.[37] Relatively, the BZO 1D-APC/YBCO interface may be more efficient for Ca diffusion due to the presence of defects, such as dislocations, on the interface, allowing Ca diffusion to extend to BZO/YBCO layers of large thicknesses along the BZO 1D-APC/YBCO interface.[38,39] Similarly, the EDS maps of Ca, Zr, and Y on the 6% ML (600 nm) sample in Fig. 2(b) are exhibited in Figs. 2(g)–2(i). Interestingly, Ca is shown to have a considerably higher concentration in the two CaY-123 spacers than in the BZO/YBCO layers, indicating again only the amount of Ca diffusing out of the spacers into the BZO/YBCO layers is moderate, which is preferred to minimize significant reduction of T_c via Ca/Y replacement[37] while facilitate Ca/Cu replacement on the Cu–O planes of YBCO lattice near the BZO 1D-APC/YBCO interface for the benefit of interface lattice mismatch via c-axis elongation of the YBCO near the interface.[26,27] Also included in Table I are the c-axis lattice constants measured on 6% ML samples of different thicknesses using XRD θ–2θ scans. The values are in the range of 11.77 to 11.72 Å, which are comparable to 11.73 Å for the 6% SL (300 nm) reference sample.

Figure 3 shows $J_c(B)$ curves measured on four 6% ML films of different thicknesses of 150 nm [Fig. 3(a)], 450 nm [Fig. 3(b)], 750 nm [Fig. 3(c)], and 1000 nm [Fig. 3(d)], respectively, at B//c in the field range of 0–9.0 T at temperatures of 50, 65, 68, 74, 77, and

TABLE I. Summary of properties of 6% BZO/YBCO ML films with variable thickness in the range of 150–1000 nm. All ML samples have five-layer structures schematically shown in Figs. 1(b) and 1(c). A 6% BZO/YBCO SL film of 300 nm in thickness is included for comparison.

Sample ID	T_c (K)	C-lattice constant (A)	$F_{p,max}$ (GN/m^3) at 65 K	J_c (MA cm^{-2}) at 65 K, 9 T (B//c)	J_c (MA cm^{-2}) at 50 K, 9 T (B//c)
6% SL (300 nm)	86.5	11.73	82.4	0.527	1.82
6% ML (150 nm)	84.0	11.77	158	1.69	2.48
6% ML (300 nm)	83.5	11.73	123	1.30	1.69
6% ML (450 nm)	86.0	11.74	130	1.33	3.57
6% ML (600 nm)	83.0	11.73	99.1	0.785	2.44
6% ML (750 nm)	85.0	11.76	111	1.25	3.72
6% ML (1000 nm)	84.5	11.72	110	1.24	3.58

81 K. Overall, all four ML samples have high J_c values while more noticeable differences are present at higher temperatures. It should be noted that the T_c values are comparable at 84, 86, 85, and 84.5 K, respectively, for the 150, 450, 750, and 1000 nm thick ML samples (Table I). Therefore, the moderate differences, especially the better J_c(B) in thicker ML samples, may not be explained by the T_c effect. Moreover, the thicker ML samples outperform their thinner counterparts at high fields and low temperatures. For example, at 50 K and 9.0 T, the J_c values of 3.57, 3.72, and 3.58 MA/cm^2, respectively, were observed for the 450, 750, and 1000 nm thick BZO/YBCO ML films, which are considerably higher than 2.48 MA/cm^2 for the 6% ML (150 nm) sample (Table I).

Figures 4(a)–4(c) present a comparison of the $J_c(B)$ curves of the same four 6% BZO/YBCO ML films of different film thicknesses of 150 nm (black), 450 nm (red), 750 nm (blue), and 1000 nm (purple) at 77, 65, and 50 K, respectively. For comparison, the $J_c(B)$ curves of a reference 6% BZO/YBCO SL sample of 150 nm in the thickness are also included in Figs. 4(a) and 4(b) (open black). Compared to its ML counterpart of the same thickness (solid black), the $J_c(B)$ values of the two sample are

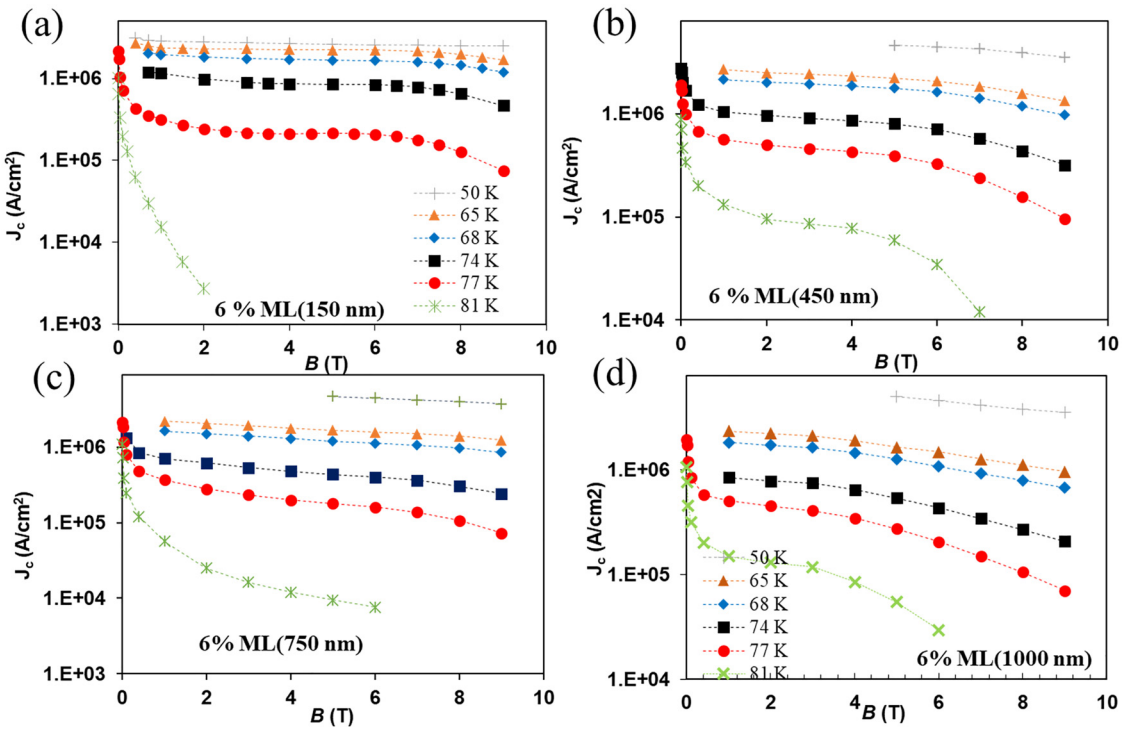

FIG. 3. J_c(B) curves measured at temperatures of 50–81 K on 6% BZO/YBCO ML films of nominal thicknesses of (a) 150, (b) 450, (c) 750, and (d) 1000 nm, respectively. The J_c measurements were taken at the B//c-axis.

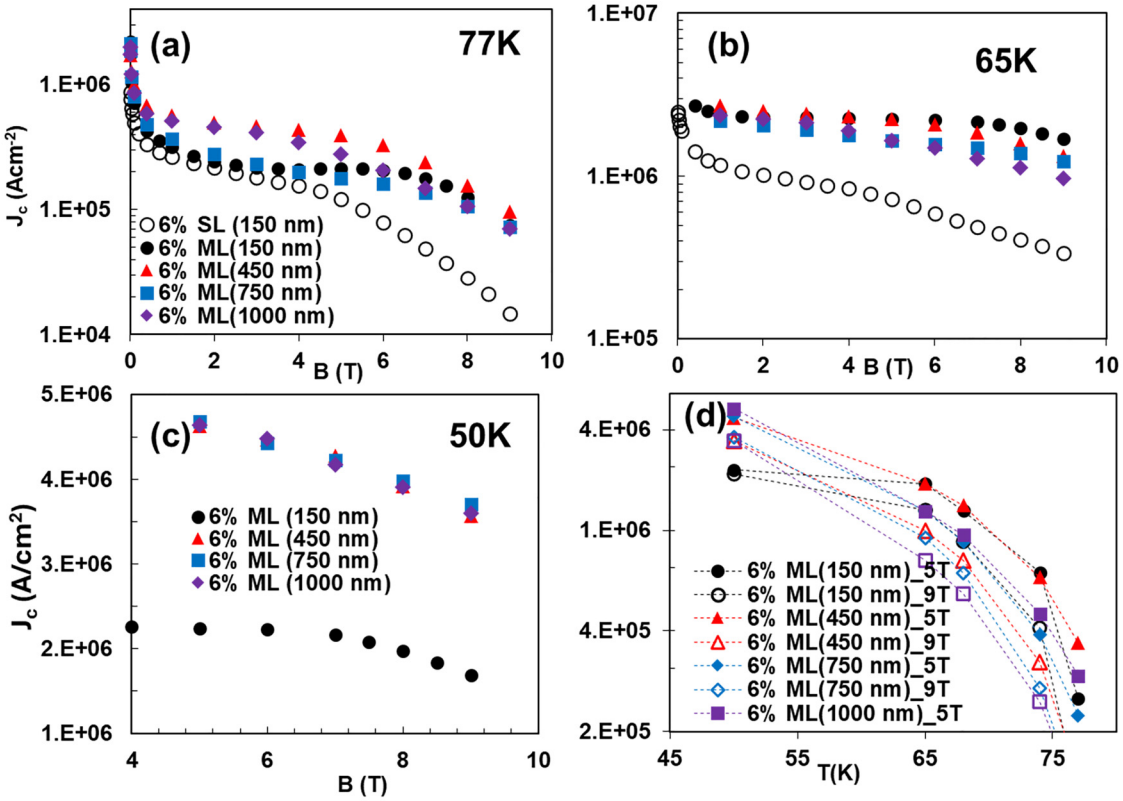

FIG. 4. $J_c(B)$ comparison of 6% BZO/YBCO ML samples of different thicknesses of 150 nm (black), 450 nm (red), 750 nm (blue), and 1000 nm (purple) at (a) 77, (b) 65, and (c) 50 K, respectively. $J_c(B)$ curves measured on a reference 6% BZO/YBCO SL sample (open black) has also been included in (a) and (b). (d) J_c (T) at 5.0 T (solid) and 9.0 T (open) of the same four ML samples in (a)–(c).

comparable at 77 K and fields ~3.0 T or lower while the ML sample exhibits considerably higher $J_c(B)$ values at B > 3.0 T and the $J_c(B)$ enhancement increases with increasing field. At 9.0 T, the $J_c(B)$ enhancement is about one order of magnitude, suggesting the improved pinning in the ML sample. At 65 K, the similar trend of the enhanced $J_c(B)$ in the ML sample can be observed in the entire range of the magnetic fields. Overall, high and comparable $J_c(B)$ values are demonstrated on the four ML samples within a factor of 2–4 across in the B field range of 0–9.0 T as the film thickness is varied in the range of 150–1000 nm. No obvious trend is observed on the thickness dependence of $J_c(B)$. For example, at 77 K, subtle differences of the J_c values for the four ML samples are mainly at lower B fields below 6–7 T. In contrast, at 65 K, the differences of the J_c values appear at higher B fields. Specifically, the J_c values at $B = 9.0$ T are 1.69, 1.33, 1.25, and 1.24 MA/cm^2, respectively, for the ML samples of 150 nm (black), 450 nm (red), 750 nm (blue), and 1000 nm (purple) in thickness. These J_c values are remarkable when compared to results from the literature reported APC/REBCO nanocomposite films in the range of 0.7–0.9 MA/cm^2.[40–43] With further decrease in temperatures, the thicker ML samples exhibit higher J_c values. As shown in Fig. 4(c), the three thicker ML samples with thicknesses of 450, 750, and 1000 nm have comparable and high J_c values across the entire B field range at 50 K, which are considerably higher than that of ML (150 nm). It should be noted that the ML samples outperform the SL counterparts in terms of the J_c(B) values. At $B = 3$ T and both 77 K and 65 K, J_c values of the ML samples is up to 0.41 and 2.4 MA/cm^2, respectively, which are higher than that reported in the literature.[42,44–50] For instance, YBCO films with surface decoration using CeO_2 and a BZO-doped YBCO film or with a 30% Y-rich precursor have J_c values of 0.12–0.13 and 0.7–1.5 MA/cm^2, respectively, at 3 T and at 77 and 65 K, respectively.[49,50] Figure 4(d) shows J_c vs temperature curves at 5.0 T (solid) and 9.0 T (open) for the same four ML samples. The decreasing J_c trend with increasing temperature is clearly observable in all the films at both fields as anticipated while the crossing of the J_c(T) curves for thin and thick ML samples is associated to the higher $J_c(B)$ at lower Ts for the latter. The increasing temperature susceptibility of J_c with increasing temperature is attributed to T approaching T_c.

Figures 5(a)–5(c) display the $F_p(B)$ curves for the same set of four 6% BZO/YBCO ML films of different thicknesses in Fig. 4 at 77, 65, and 50 K. At higher temperatures, the $F_p(B)$ curves exhibit a

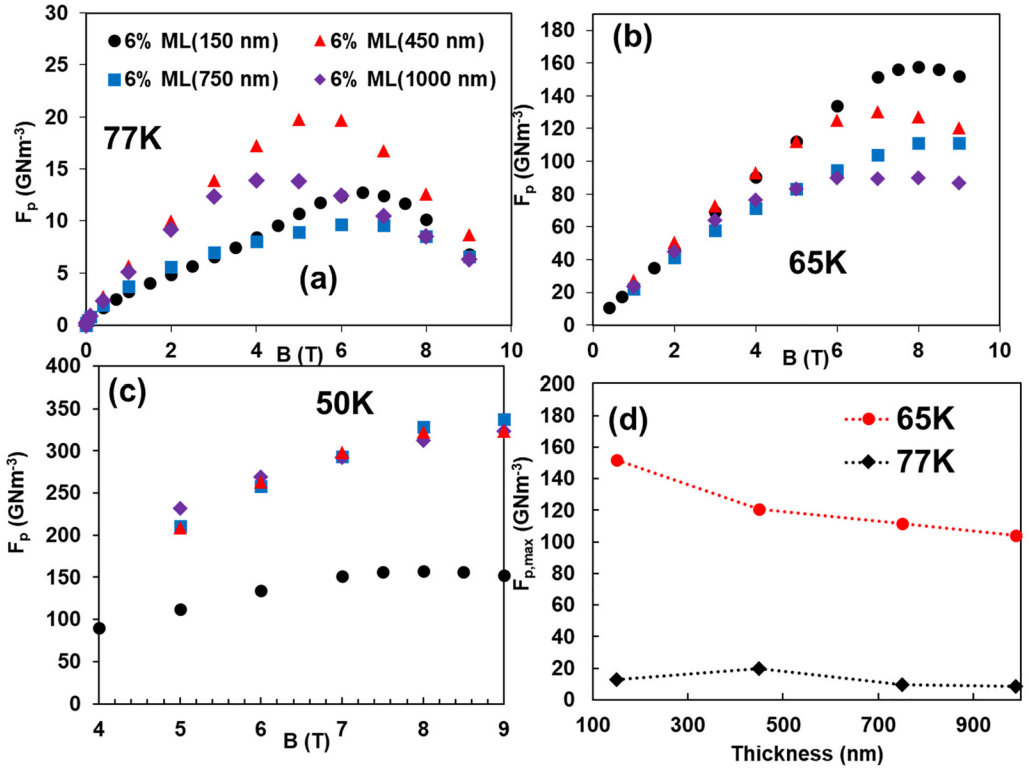

FIG. 5. F_p(B) comparison of 6% BZO/YBCO ML samples of different thicknesses of 150 nm (black), 450 nm (red), 750 nm (blue), and 1000 nm (purple) at (a) 77, (b) 65, and (c) 50 K, respectively; and (d) $F_{p,max}$ as a function of ML film's thickness at 65 K (red) and 77 K (black).

bell-shape and the value of $F_p(B)$ at the peak location of B_{max} is defined as $F_{p,max}$. At 77 K, the $F_{p,max}$ values are 13, 20, 4.8, 11, and 14 GNm^{-3} for 150 nm (black), 450 nm (red), 750 nm (blue), and 1000 nm (purple) thick ML films, respectively [Fig. 5(a)]. Again, there seems to be no trend in the $F_{p,max}$ values vs sample thickness. At 65 K, the 150 nm ML sample has the highest $F_{p,max} \sim 158$ GNm^{-3}, which is followed with 130, 111, and 110 GNm^{-3} for the 450, 750, and 1000 nm ML films, respectively [Fig. 5(b) and Table I]. It should be noted that the $F_{p,max} \sim 82$ GNm^{-3} for the reference 6% SL (300 nm) samples is considerably lower at 65 K (Table I).[23] The enhanced $F_{p,max}$, as well as the B_{max} values ranging from 7.0 to 9.0 T for the four ML samples in contrast to ~5.0 T in the 6% SL (150 nm),[27–30] illustrate the benefit of Ca ion diffusion in the BZO/YBCO ML samples. Nevertheless, the B_{max} values in the ML samples are still lower than the accommodation field $B^* \sim 14.3$ T estimated from the areal density of the BZO 1D-APCs in 6% BZO/YBCO nanocomposite samples, suggesting a considerable portion of the BZO 1D-APCs generated need to be activated for further improved pinning at 65 K. With further decrease of the temperature to 50 K, the $F_{p,max}$ could not be determined since F_p(B) increases monotonically with increasing B in the range of 0–9.0 T, which means $B_{max} > 9.0$ T. Nevertheless, the overall high $F_p(B)$ values were observed on all 6% BZO/YBCO ML samples. At 50 K, the highest F_p value of 337 GNm^{-3} was obtained at $B = 9.0$ T in the ML samples. These values are larger than the 80–140 GNm^{-3} reported on 120–220 nm thick BZO/YBCO SL films,[51,52] illustrating the benefit of the ML approach in enhancing J_c and pinning in thicker films. Figure 5(d) summarizes the data. It shows $F_{p,max}$ measured at 65 K (red) and 77 K (black) as a function of the ML film thickness. The fact of comparable $F_{p,max}$ values obtained on the ML samples of different thicknesses suggests that the diffusion of Ca ions is fairly effective through a large BZO/YBCO thickness in the five-layer ML structure.

Figures 6(a)–6(d) compare the $J_c(\theta)$ curves of the same four 6% ML films of different thicknesses in Fig. 4 at 77 and 65 K and several selected magnetic fields. Two peaks at θ around 0° (B//c) and 90° (B//ab) can be clearly seen in all samples. The former corresponds to the enhanced pinning by the BZO 1D-APCs, while the latter, the intrinsic pinning by ab-planes in YBCO. The 6% ML (450 nm) film has the highest J_c values and lowest J_c anisotropy in the entire angular range at 77 K and 3.0 and 5.0 T magnetic fields. In contrast, the 150 nm ML film has the lowest $J_c(\theta)$ values as compared to the thicker ML films although it outperforms its SL counterpart considerably.[26] Interestingly, the differences between the $J_c(\theta)$ values of the four ML samples with different thicknesses reduce at lower temperature of 65 K. Furthermore, the correlated pinning by the BZO 1D-APCs is stronger in all ML films as compared to the intrinsic pinning at the B//ab-plane as exhibited by the

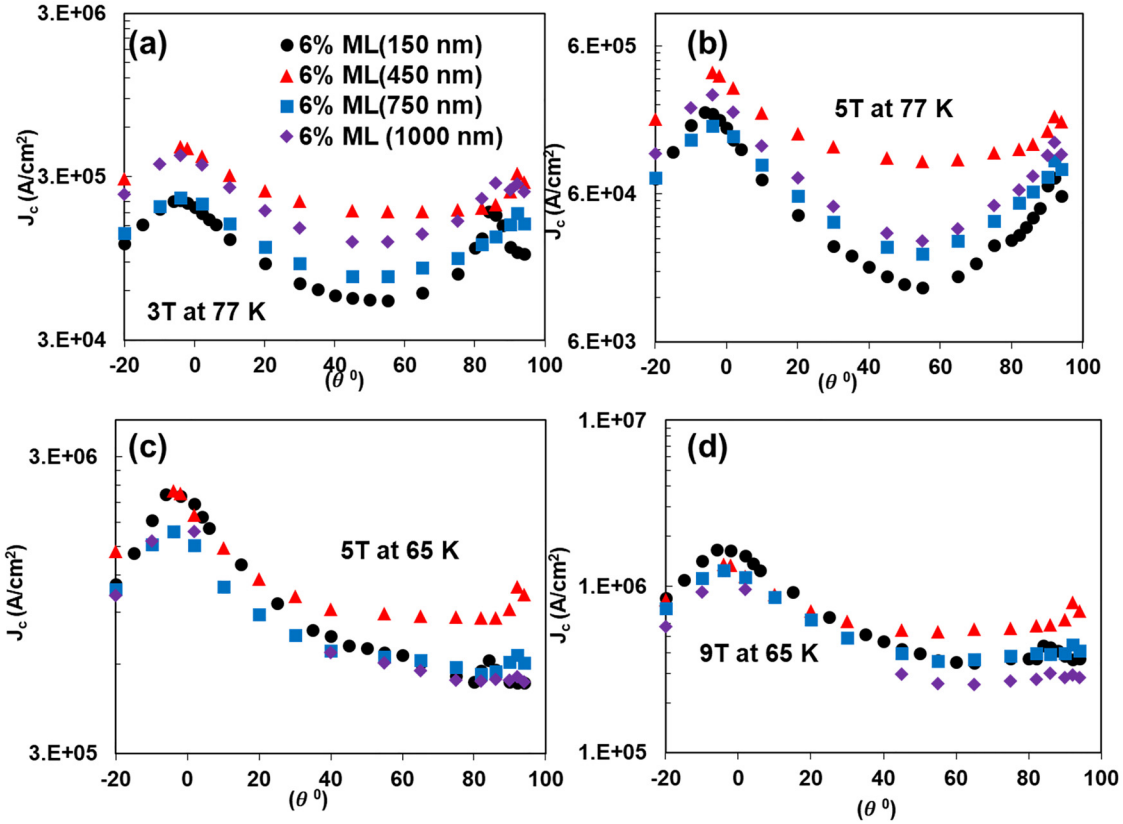

FIG. 6. $J_c(\theta)$ comparison of 6% BZO/YBCO ML films of different thicknesses of 150 nm (black), 450 nm (red), 750 nm (blue), and 1000 nm (purple) at (a) 77 K, 3.0 T, (b) 77 K and 5.0 T, (c) 65 K and 5.0 T, and (d) 65 K and 9.0 T, respectively.

higher peak value of $J_c(\theta)$ around $\theta \sim 0°$ than at $\theta \sim 90°$ at 65 K. At 5.0 T, the ratio between these two peaks is in the range of 2.1–2.3 at 5.0 T and it is around 1.8–4.1 at 9.0 T.

Figures 7(a) and 7(b) compare the $J_c(\theta)$ curves of 6% ML films of thicknesses of 450 nm (red), 750 nm (blue), and 1000 nm (purple) with that of a reference 6% SL sample of 300 nm in thickness (black) at temperatures of 50 and 30 K, respectively, in magnetic field of 9.0 T. Note the 6% SL (300 nm) sample is included for comparison because J_c in undoped and BZO/YBCO SL films decreases monotonically with the thickness.[53] While BZO 1D-APCs are shown to reduce the thickness dependence, the highest J_c is observed in undoped and BZO/YBCO SL films of thickness 150–300 nm.[54,55] Almost in the entire θ range, the ML samples have higher $J_c(\theta)$ than their SL counterpart. At 50 K and 9.0 T, for example, the peak $J_c \sim 3.6$–3.7 MA/cm^2 for the 750 and 1000 nm ML samples at the B//c-axis is twice of that (1.8 MA/cm^2) for the SL film [Fig. 7(a)]. In addition, the ratio between the $J_c(\theta)$ peaks at $\theta = 0°$ (B//c) and $\theta = 90°$ (B//ab) is in the range of 1.1–1.2 at 9.0 T for the ML samples while it is ~0.9 for the SL sample. The higher J_c values and higher $J_c(\theta = 0°)/J_c(\theta = 90°)$ ratios in the ML samples can be attributed to the Ca diffusion induced pinning enhancement of BZO 1D-APCs. With further decreasing temperature to 30 K, the $J_c(\theta)$ peak ratios for all ML and SL samples become comparable at ~0.72 [Fig. 7(b)], indicating more effective intrinsic pinning at low temperatures and high fields. Despite comparable $J_c(\theta)$ peak values for the ML and SL samples at $\theta = 0°$ (B//c) and $\theta = 90°$ (B//ab), the ML samples have considerably reduced J_c anisotropy with respect to the orientation of B field. This means the benefit of enhanced pinning by Ca diffusion in the ML samples at higher temperatures of 65–77 K (Fig. 6) can be extended to lower temperatures. As shown in Fig. 7(b), the maximum and minimum $J_c(\theta)$ values are 5.7 MA/cm^2 (at $\theta = 90°$ or B//ab) and 3.1 MA/cm^2 (at $\theta \sim 30°$), respectively, for the ML samples at 30 K and 9.0 T, which yield J_c anisotropy estimated from the ratio of $(J_{c,max} - J_{c,min})/J_{c,min}$ to be 84%. For the 6% SL (300 nm) sample in Fig. 7(b), the maximum and minimum $J_c(\theta)$ values are 5.5 MA/cm^2 (at $\theta = 90°$ or B//ab) and 2.1 MA/cm^2 (at $\theta \sim 30°$), respectively, leading to higher J_c anisotropy or smaller ratio of $(J_{c,max} - J_{c,min})/J_{c,min}$ around 160%.

Figure 8(a) exhibits the J_c vs film thickness curves measured on 6% BZO/YBCO ML films at $B = 9.0$ T (B//c-axis) and 65 K (red) and 50 K (blue), respectively. At 65 K, a moderate drop of J_c values was observed with increasing thickness from 1.67 MA/cm^2 at 150 nm to 1.24 MA/cm^2 at 1000 nm thickness. Interestingly, this

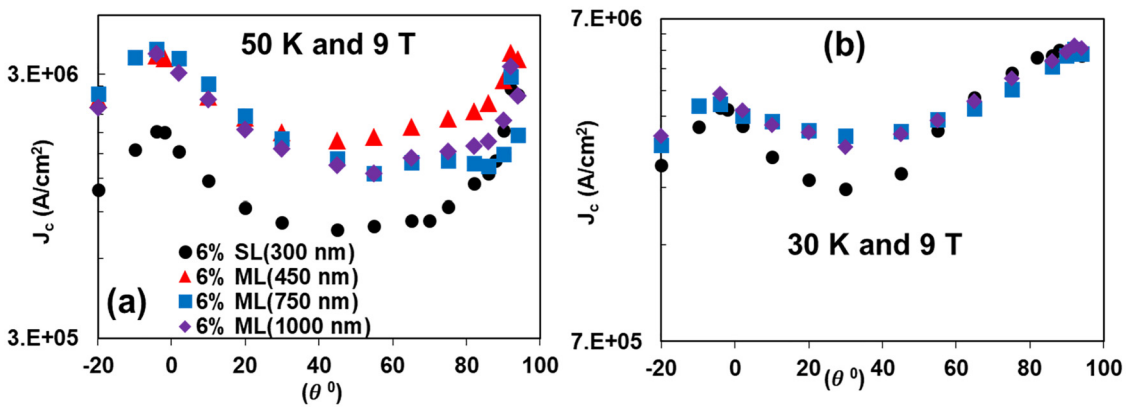

FIG. 7. $J_c(\theta)$ comparison of 6% BZO/YBCO ML films of different thicknesses of 450 nm (red), 750 nm (blue), and 1000 nm (purple) at (a) 50 K, 9.0 T and (b) 30 K and 9.0 T. A 300 nm thick 6% BZO/YBCO SL sample (black) is also included for comparison.

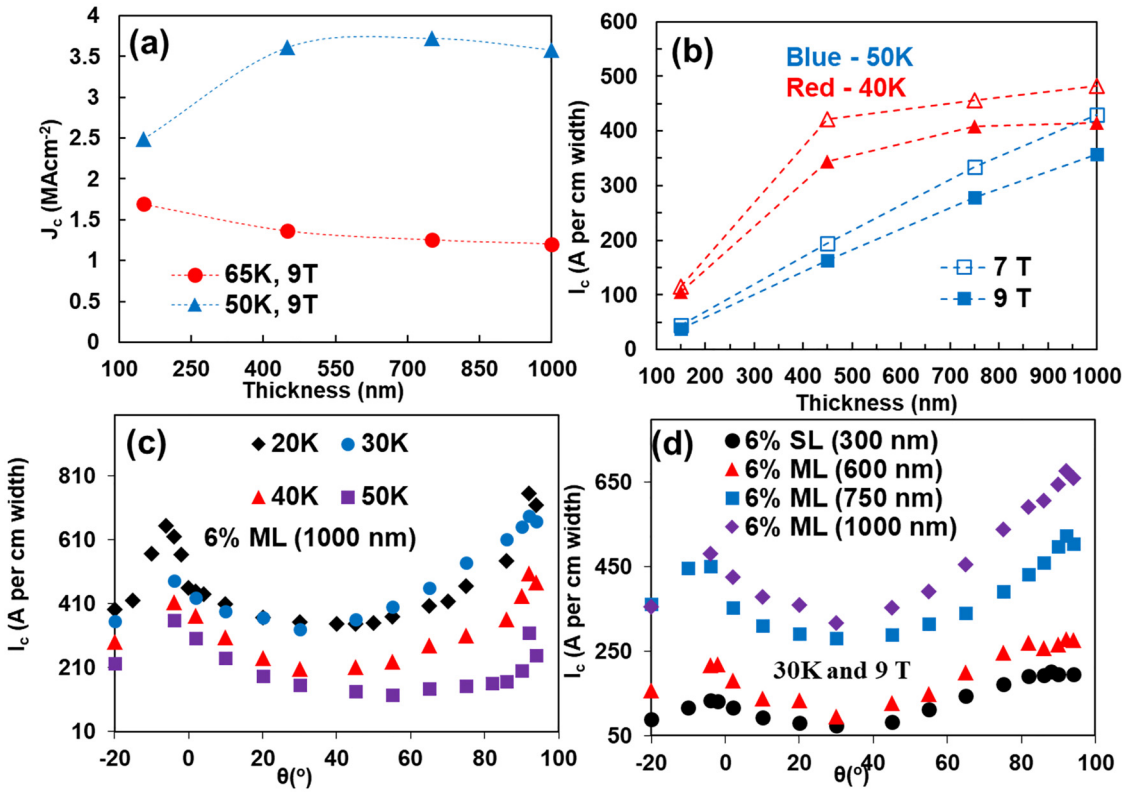

FIG. 8. (a) Film thickness dependence of J_c of 6% BZO/YBCO ML films at 65 and 50 K and 9.0 T (*B*//c). (b) I_c per cm-width as a function of the thickness of the ML films at 50 K (blue) and 40 K (red) and 7.0 T (open) and 9.0 T (solid). The B//c-axis was in all measurements. I_c per cm-width at 9.0 T measured on (c) the 6% ML (1000 nm) film as a function of θ at temperatures of 20–50 K, and (d) 6% ML (600 nm), 6% ML (750 nm), and 6% ML (1000 nm) samples in comparison with the 6% SL (300 nm) counterparts.

trend is altered at the lower temperature of 50 K as an increase of J_c appears at larger film thickness above ~450 nm. Specifically at 50 K and 9.0 T, the 6% ML (150 nm) sample has $J_c \sim 2.48$ MA/cm^2, which is increased to 3.61 MA/cm^2 for the 6% ML (450 nm) sample, above which the J_c values exhibit almost no thickness dependence. This is desired for practical applications at low temperatures and high fields that require high I_c. Figure 8(b) shows the thickness dependence of the I_c per cm-width at 50 K (blue) and 40 K (red) in B fields of 7.0 T (dash) and 9.0 T (solid), respectively, at B//c-axis. Overall, I_c increases approximately linearly with the ML film thickness at 50 K. At lower temperature of 40 K, the I_c vs thickness curves become more nonlinear due to the increase of J_c value with increasing thickness and hence a larger increase of I_c with the thickness in thicker ML samples. Specifically, at 7.0–9.0 T, the I_c increases by a factor 2.7–3.6 as the ML thickness increases from 150 to 1000 nm at 40–50 K reaching to 360–480 A per cm-width desired for practical applications.[56,57]

Figure 8(c) exhibits the $I_c(\theta)$ per cm-width curves of the 6% ML (1000 nm) film at 9.0 T and low temperatures of 20–50 K. Interestingly, the peaks of I_c at both $\theta = 0$ (B//c) and =90° (B//ab) are clearly visible at all temperatures. The former indicates the correlated pinning by BZO 1D-APCs remains effective at low temperatures and the latter is associated to the intrinsic pinning of YBCO. With decreasing temperatures, the amplitudes of the two peaks switch positions from a higher I_c peak by BZO 1D-APC pinning at higher temperatures to a higher I_c peak by the intrinsic pinning at lower temperatures. At 50 K, the I_c peak by BZO 1D-APCs is ~359 A/cm-width which is 1.1 times of that by the intrinsic pinning. At 20 K, the I_c peak at B//c by BZO 1D-APCs is ~654 A/cm-width while that by the intrinsic pinning is 1.15 times higher at 753 A/cm-width. However, both peaks seem to be broad in a wide θ range at lower temperatures, which is beneficial to reduce the I_c anisotropy $I_{c,min}/I_{c,max}$ estimated to be 0.35 at 50 K to 0.44 at 20 K. Figure 8(d) compares the $I_c(\theta)$ per cm-width curves of the 600, 750, and 1000 nm thick 6% BZO/YBCO ML films and the 300 nm thick SL reference film at 9.0 T and 30 K. Besides the high $I_c(\theta)$ proportional to the thickness due to comparable J_c for ML samples of different thicknesses, an interesting difference between ML samples and SL counterpart is in the ratio between the two I_c peaks by BZO 1D-APC pinning and the intrinsic pinning. In contrast to I_c (B//ab)/I_c (B//c) ~ 1.5 for the SL sample, smaller ratios of 1.3–1.4 were observed for the ML samples, illustrating the enhanced pinning of the BZO 1D-APCs due to Ca ion diffusion.

IV. CONCLUSION

In summary, this work reports an exploratory study of microstructure and superconducting properties on the 6% BZO/YBCO ML films of variable thickness in the range of 150–1000 nm. The same five-layer structure was employed with two CaY-123 spacers of 10 nm in thickness to enable Ca ion diffusion from the spacers into the three BZO/YBCO layers each having a thickness varied from 50 to 330 nm. A few interesting insights have been obtained in this study. First, the five-layer may provide a scheme to introduce a small amount of Ca ions into BZO/YBCO layers by diffusing Ca from 10 nm thick CaY-123 spacers to BZO/YBCO of a layer thickness up to 330 nm. Second, the amount of the diffused Ca is small as suggested by the TEM/EDS study as a significant amount of Ca remains in the CaY-123 spacers. Third, the effect of the diffused Ca ions in BZO/YBCO layers is illustrated in the high J_c obtained in a wide temperature range of 20–80 K at magnetic fields up 9.0 T, confirming a large improvement of pinning in the ML samples as compared to their SL counterparts. Finally, and more interestingly, with decreasing temperatures and increasing B field, the J_c improvement is more significant in thicker ML films as illustrated in the increasing J_c with the ML film thickness together with decreasing J_c anisotropy with respect to the orientations of B fields. This leads to large I_c values in the 6% BZO/YBCO ML films. At 20 K and 9.0 T, the I_c is up to 654 A/cm-width at B//c in the 6% ML (1000 nm) sample, which is close to 753 A/cm-width at B//ab due to the intrinsic pinning. The high performance of the 6% ML BZO/YBCO thick films illustrates the efficacy of Ca ion diffusion through a large BZO/YBCO layer thickness, suggesting further enhanced pinning of BZO 1D-APCs may be achieved through engineering the microstructure of the BZO/YBCO nanocomposites.

ACKNOWLEDGMENTS

This research was supported in part by NSF (Contract Nos. NSF-DMR-1909292, 2413044, and NSF-ECCS-2314401, the AFRL Aerospace Systems Directorate, the Air Force Office of Scientific Research (LRIR Nos. 18RQCOR100, 23RQCOR008, and 24RQCOR004). J. S. and H.W. acknowledge the support from the U.S. Office of Naval Research (ONR, No. N00014-20-1-2600) and the U.S. National Science Foundation (No. DMR-2016453) for the TEM/STEM work.

AUTHOR DECLARATIONS

Conflict of Interest

The authors have no conflicts to disclose.

Author Contributions

Victor Ogunjimi: Data curation (equal); Formal analysis (equal); Writing – original draft (equal); Writing – review & editing (equal). **Mohan Panth:** Data curation (equal); Formal analysis (equal); Writing – original draft (equal); Writing – review & editing (equal). **Mary Ann Sebastian:** Conceptualization (equal); Data curation (equal); Formal analysis (equal); Writing – review & editing (equal). **Jianan Shen:** Data curation (equal); Formal analysis (equal); Writing – review & editing (equal). **Matteo Moceri:** Data curation (equal); Formal analysis (equal); Writing – review & editing (equal). **Charles Ebbing:** Data curation (equal); Formal analysis (equal); Writing – review & editing (equal). **Timothy Haugan:** Conceptualization (equal); Funding acquisition (equal); Writing – review & editing (equal). **Haiyan Wang:** Conceptualization (equal); Funding acquisition (equal); Writing – review & editing (equal). **Aafiya:** Data curation (equal); Formal analysis (equal); Writing – review & editing (equal). **Judy Wu:** Conceptualization (equal); Funding acquisition (equal); Writing – original draft (equal); Writing – review & editing (equal).

DATA AVAILABILITY

The data that support the findings of this study are available from the corresponding author upon reasonable request.

REFERENCES

[1]N. Long, R. Badcock, K. Hamilton, A. Wright, Z. Jiang, and L. Lakshmi, "Development of YBCO Roebel cables for high current transport and low AC loss applications," J. Phys.: Conf. Ser. **234**, 022021 (2010).

[2]W. Schmidt, H.-P. Kraemer, H.-W. Neumueller, U. Schoop, D. Verebelyi, and A. P. Malozemoff, "Investigation of YBCO coated conductors for fault current limiter applications," IEEE Trans. Appl. Supercond. **17**(2), 3471–3474 (2007).

[3]Y. Zhao, J. Wang, S. Wang, Z. Ren, H. Song, X. Wang, and C. Cheng, "Applications of YBCO melt textured bulks in Maglev technology," Physica C **412–414**, 771–777 (2004).

[4]M. W. Rupich, D. T. Verebelyi, W. Zhang, T. Kodenkandath, and X. Li, "Metalorganic deposition of YBCO films for second-generation high-temperature superconductor wires," MRS Bull. **29**(8), 572–578 (2004).

[5]B. Goodman, "Type II superconductors," Rep. Prog. Phys. **29**(2), 445 (1966).

[6]N. Khare, *Handbook of High-Temperature Superconductor* (CRC Press, 2003).

[7]D. Larbalestier, A. Gurevich, D. M. Feldmann, and A. Polyanskii, "High-Tc superconducting materials for electric power applications," Nature **414**(6861), 368–377 (2001).

[8]X. Obradors, T. Puig, S. Ricart, A. Palau, M. Coll, J. Gutiérrez, J. Farjas, and E. Bartolomé, "Progress in superconducting $REBa_2Cu_3O_7$ (RE = rare earth) coated conductors derived from fluorinated solutions," Supercond. Sci. Technol. **37**(5), 053001 (2024).

[9]D. Huang, H. Gu, H. Shang, T. Li, B. Xie, Q. Zou, D. Chen, W.-K. Chu, and F. Ding, "Enhancement in the critical current density of $BaTiO_3$-doped YBCO films by low-energy (60 keV) proton irradiation," Supercond. Sci. Technol. **34**(4), 045001 (2021).

[10]S. Kang, A. Goyal, J. Li, A. A. Gapud, P. M. Martin, L. Heatherly, J. R. Thompson, D. K. Christen, F. List, M. Paranthaman, and D. F. Lee, "High-performance high-Tc superconducting wires," Science **311**(5769), 1911–1914 (2006).

[11]S. Foltyn, Q. Jia, P. Arendt, L. Kinder, Y. Fan, and J. Smith, "Relationship between film thickness and the critical current of $YBa_2Cu_3O_{7-\delta}$-coated conductors," Appl. Phys. Lett. **75**(23), 3692–3694 (1999).

[12]S. Foltyn, H. Wang, L. Civale, Q. Jia, P. Arendt, B. Maiorov, Y. Li, M. Maley, and J. L. MacManus-Driscoll, "Overcoming the barrier to 1000 A/cm width superconducting coatings," Appl. Phys. Lett. **87**(16), 162505 (2005).

[13]R. Emergo, J. Wu, T. Aytug, and D. Christen, "Thickness dependence of superconducting critical current density in vicinal $YBa_2Cu_3O_{7-\delta}$ thick films," Appl. Phys. Lett. **85**(4), 618–620 (2004).

[14]T. Matsushita, "Flux pinning in superconducting 123 materials," Supercond. Sci. Technol. **13**(6), 730–737 (2000).

[15]K. Matsumoto and P. Mele, "Artificial pinning center technology to enhance vortex pinning in YBCO coated conductors," Supercond. Sci. Technol. **23**(1), 014001 (2010).

[16]J. Wu, M. Panth, V. Ogunjimi, B. Gautam, J. Shi, M. A. Sebastian, T. Haugan, C. Ebbing, D. Zhang, J. Jian, J. Huang, Y. Zhang, and H. Wang, "Artificial pinning centers and the quest of high critical current densities in HTS nanocomposites," IEEE Trans. Appl. Supercond. **33**(5), 1–6 (2023).

[17]J. MacManus-Driscoll, S. Foltyn, Q. Jia, H. Wang, A. Serquis, L. Civale, B. Maiorov, M. Hawley, M. Maley, and D. Peterson, "Strongly enhanced current densities in superconducting coated conductors of $YBa_2Cu_3O_{7-x}$ + $BaZrO_3$," Nat. Mater. **3**(7), 439 (2004).

[18]J. Wu and J. Shi, "Interactive modeling-synthesis-characterization approach towards controllable *in situ* self-assembly of artificial pinning centers in RE-123 films," Supercond. Sci. Technol. **30**(10), 103002 (2017).

[19]S. Miura, Y. Yoshida, Y. Tsuchiya, Y. Ichino, S. Awaji, A. Ichinose, K. Matsumoto, A. Ibi, T. Izumi, and M. Iwakuma, "Strongly enhanced irreversibility field and flux pinning force density in $SmBa_2Cu_3O$ y-coated conductors with well-aligned $BaHfO_3$ nanorods," Appl. Phys. Express **10**(10), 103101 (2017).

[20]S. Chen, M. A. Sebastian, B. Gautam, J. Wilt, Y. Chen, L. Sun, Z. Xing, T. Haugan, and J. Wu, "Generating mixed morphology $BaZrO_3$ artificial pinning centers for strong and isotropic pinning in $BaZrO_3$–Y_2O_3 double-doped YBCO thin films," Supercond. Sci. Technol. **30**(12), 125011 (2017).

[21]P. Mele, K. Matsumoto, T. Horide, A. Ichinose, M. Mukaida, Y. Yoshida, S. Horii, and R. Kita, "Ultra-high flux pinning properties of $BaMO_3$-doped $YBa_2Cu_3O_{7-x}$ thin films (M = Zr, Sn)," Supercond. Sci. Technol. **21**(3), 032002 (2008).

[22]B. Gautam, M. A. Sebastian, S. Chen, J. Shi, T. Haugan, Z. Xing, W. Zhang, J. Huang, H. Wang, M. Osofsky, J. Prestigiacomo, and J. Z. Wu, "Transformational dynamics of BZO and BHO nanorods imposed by $Y2O_3$ nanoparticles for improved isotropic pinning in $YBa_2Cu_3O_{7-\delta}$ thin films," AIP Adv. **7**(7), 075308 (2017).

[23]B. Gautam, M. A. Sebastian, S. Chen, S. Misra, J. Huang, F. Javier Baca, R. Emergo, T. Haugan, Z. Xing, H. Wang, and J. Z. Wu, "Probing the effect of interface on vortex pinning efficiency of one-dimensional $BaZrO_3$ and $BaHfO_3$ artificial pinning centers in $YBa_2Cu_3O_{7-x}$ thin films," Appl. Phys. Lett. **113**(21), 212602 (2018).

[24]S. Chen, M. A. Sebastian, B. Gautam, J. Wilt, T. Haugan, Z. Xing, and J. Wu, "Enhancement of isotropic pinning force in YBCO films with $BaZrO_3$ nanorods and $Y2O_3$ nanoparticles," IEEE Trans. Appl. Supercond. **27**(4), C4 (2017).

[25]E. Galstyan, R. Pratap, M. Paidpilli, G. Majkic, and V. Selvamanickam, "Pinning characteristics of Zr and Hf-added REBCO coated conductors made by advanced MOCVD in low-to-high magnetic fields," IEEE Trans. Appl. Supercond. **31**(5), 1–5 (2021).

[26]V. Ogunjimi, M. A. Sebastian, D. Zhang, B. Gautam, J. Jian, J. Huang, Y. Zhang, T. Haugan, H. Wang, and J. Wu, "Enhancing magnetic pinning by $BaZrO_3$ nanorods forming coherent interface by strain-directed Ca-doping in $YBa_2Cu_3O_{7-x}$ nanocomposite films," Supercond. Sci. Technol. **34**(10), 104002 (2021).

[27]J. Z. Wu, V. Ogunjimi, M. A. Sebastian, D. Zhang, J. Jian, J. Huang, Y. Zhang, B. Gautam, T. Haugan, and H. Wang, "Enabling coherent $BaZrO_3$ nanorods/$YBa_2Cu_3O_{7-x}$ interface through dynamic lattice enlargement in vertical epitaxy of $BaZrO_3$/$YBa_2Cu_3O_{7-x}$ nanocomposites," Supercond. Sci. Technol. **35**(3), 034001 (2022).

[28]V. Ogunjimi, M. Panth, M. A. Sebastian, D. Zhang, T. Haugan, H. Wang, and J. Wu, "Probing effect of strain field on Ca diffusion in $BaZrO_3$-doped $YBa_2Cu_3O_{7-x}$/$Ca_{0.3}Y_{0.7}Ba_2Cu_3O_{7-x}$ multilayer nanocomposite films," Physica C **601**, 1354111 (2022).

[29]M. Panth, M. A. Sebastian, D. Zhang, V. Ogunjimi, B. Gautam, J. Jian, J. Huang, Y. Zhang, T. Haugan, H. Wang, and J. Wu, "Multilayer $YBa_2Cu_3O_{7-x}$/$Ca_{0.3}Y_{0.7}Ba_2Cu_3$ O_{7-x} nanocomposite films with 2–8% $BaZrO_3$ doping for high-field applications," IEEE Trans. Appl. Supercond. **32**(8), 1–8 (2022).

[30]M. Panth, V. Ogunjimi, M. A. Sebastian, B. Gautam, T. Haugan, and J. Wu, "The benefit of Ca in improving pinning of $BaZrO_3$–Y_2O_3 doubly-doped $YBa_2Cu_3O_{7-x}$/$Ca_{0.3}Y_{0.7}Ba_2Cu_3O_{7-x}$ multilayer nanocomposite films," Mater. Res. Express **10**(4), 046001 (2023).

[31]M. A. P. Sebastian, J. N. Reichart, M. M. Ratcliff, T. J. Bullard, J. L. Burke, C. R. Ebbing, G. Y. Panasyuk, C.-F. Tsai, W. Zhang, J. Huang, H. Wang, J. Wu, and T. J. Haugan, "Study of the flux pinning landscape of YBCO thin films with single and mixed phase additions $BaMO_3$ + Z: M = Hf, Sn, Zr and Z = Y_2O_3, Y211," IEEE Trans. Appl. Supercond. **27**(4), 1–5 (2017).

[32]J. Wu, J. Shi, F. Baca, R. Emergo, J. Wilt, and T. Haugan, "Controlling $BaZrO_3$ nanostructure orientation in YBa_2Cu_3O films for a three-dimensional pinning landscape," Supercond. Sci. Technol. **28**(12), 125009 (2015).

[33]G. A. Daniels, A. Gurevich, and D. C. Larbalestier, "Improved strong magnetic field performance of low angle grain boundaries of calcium and oxygen over-doped $YBa_2Cu_3O_x$," Appl. Phys. Lett. **77**(20), 3251–3253 (2000).

[34]A. Schmehl, B. Goetz, R. R. Schulz, C. W. Schneider, H. Bielefeldt, H. Hilgenkamp, and J. Mannhart, "Doping-induced enhancement of the critical currents of grain boundaries in $YBa_2Cu_3O_{7-\delta}$," Europhys. Lett. **47**(1), 110 (1999).

[35]P. Alireza, G. Zhang, W. Guo, J. Porras, T. Loew, Y.-T. Hsu, G. Lonzarich, M. Le Tacon, B. Keimer, and S. E. Sebastian, "Accessing the entire overdoped regime in pristine $YBa_2Cu_3O_{6+x}$ by application of pressure," Phys. Rev. B **95**(10), 100505 (2017).
[36]R. F. Klie, J. P. Buban, M. Varela, A. Franceschetti, C. Jooss, Y. Zhu, N. D. Browning, S. T. Pantelides, and S. J. Pennycook, "Enhanced current transport at grain boundaries in high-T-c superconductors," Nature **435**(7041), 475–478 (2005).
[37]G. Hammerl, A. Schmehl, R. Schulz, B. Goetz, H. Bielefeldt, C. Schneider, H. Hilgenkamp, and J. Mannhart, "Enhanced supercurrent density in polycrystalline $YBa_2Cu_3O_{7-\delta}$ at 77 K from calcium doping of grain boundaries," Nature **407**(6801), 162–164 (2000).
[38]C. Cantoni, Y. Gao, S. H. Wee, E. D. Specht, J. Gazquez, J. Meng, S. J. Pennycook, and A. Goyal, "Strain-driven oxygen deficiency in self-assembled, nanostructured, composite oxide films," ACS Nano **5**(6), 4783–4789 (2011).
[39]T. Horide, F. Kametani, S. Yoshioka, T. Kitamura, and K. Matsumoto, "Structural evolution induced by interfacial lattice mismatch in self-organized $YBa_2Cu_3O_{7-\delta}$ nanocomposite film," ACS Nano **11**(2), 1780–1788 (2017).
[40]P. Cayado, M. Erbe, S. Kauffmann-Weiss, C. Bühler, A. Jung, J. Hänisch, and B. Holzapfel, "Large critical current densities and pinning forces in CSD-grown superconducting $GdBa_2Cu_3O_{7-x}$–$BaHfO_3$ nanocomposite films," Supercond. Sci. Technol. **30**(9), 094007 (2017).
[41]J. Gutiérrez, A. Llordés, J. Gázquez, M. Gibert, N. Romà, S. Ricart, A. Pomar, F. Sandiumenge, N. Mestres, T. Puig, and X. Obradors, "Strong isotropic flux pinning in solution-derived $YBa_2Cu_3O_{7-x}$ nanocomposite superconductor films," Nat. Mater. **6**(5), 367–373 (2007).
[42]V. Selvamanickam, M. H. Gharahcheshmeh, A. Xu, E. Galstyan, L. Delgado, and C. Cantoni, "High critical currents in heavily doped (Gd, Y) $Ba_2Cu_3O_x$ superconductor tapes," Appl. Phys. Lett. **106**(3), 032601 (2015).
[43]M. Miura, B. Maiorov, S. Baily, N. Haberkorn, J. Willis, K. Marken, T. Izumi, Y. Shiohara, and L. Civale, "Mixed pinning landscape in nanoparticle-introduced $YGdBa_2Cu_3O_y$ films grown by metal organic deposition," Phys. Rev. B **83**(18), 184519 (2011).
[44]S. Miura, Y. Tsuchiya, Y. Yoshida, Y. Ichino, S. Awaji, K. Matsumoto, A. Ibi, and T. Izumi, "Strong flux pinning at 4.2 K in $SmBa_2Cu_3O_y$ coated conductors with $BaHfO_3$ nanorods controlled by low growth temperature," Supercond. Sci. Technol. **30**(8), 084009 (2017).
[45]S. Miura, Y. Yoshida, Y. Ichino, Q. Xu, K. Matsumoto, A. Ichinose, and S. Awaji, "Improvement in J_c performance below liquid nitrogen temperature for $SmBa_2Cu_3O_y$ superconducting films with $BaHfO_3$ nano-rods controlled by low-temperature growth," APL Mater. **4**(1), 016102 (2016).
[46]V. Selvamanickam, M. H. Gharahcheshmeh, A. Xu, Y. Zhang, and E. Galstyan, "Critical current density above 15 MA cm^{-2} at 30 K, 3 T in 2.2 μm thick heavily-doped (Gd, Y) $Ba_2Cu_3O_x$ superconductor tapes," Supercond. Sci. Technol. **28**(7), 072002 (2015).
[47]D. Feldmann, T. Holesinger, B. Maiorov, S. Foltyn, J. Coulter, and I. Apodaca, "Improved flux pinning in $YBa_2Cu_3O_7$ with nanorods of the double perovskite Ba_2YNbO_6," Supercond. Sci. Technol. **23**(9), 095004 (2010).
[48]A. Goyal, S. Kang, K. J. Leonard, P. M. Martin, A. A. Gapud, M. Varela, M. Paranthaman, A. O. Ijaduola, E. D. Specht, J. R. Thompson, D. K. Christen, S. J. Pennycook, and F. A. List, "Irradiation-free, columnar defects comprised of self-assembled nanodots and nanorods resulting in strongly enhanced flux-pinning in $YBa_2Cu_3O_{7-\delta}$ films," Supercond. Sci. Technol. **18**(11), 1533 (2005).
[49]J. Nie, H. Yamasaki, H. Yamada, Y. Nakagawa, K. Develos-Bagarinao, and Y. Mawatari, "Evidence for c-axis correlated vortex pinning in Y $Ba_2Cu_3O_{7-\delta}$ films on sapphire buffered with an atomically flat CeO_2 layer having a high density of nanodots," Supercond. Sci. Technol. **17**(7), 845 (2004).
[50]A. A. Gapud, R. Feenstra, D. K. Christen, J. R. Thompson, and T. Holesinger, "Temperature and magnetic field dependence of critical currents in YBCO coated conductors with processing-induced variations in pinning properties," IEEE Trans. Appl. Supercond. **15**(2), 2578–2581 (2005).
[51]A. Crisan, M. M. Awang Kechik, P. Mikheenko, V.-S. Dang, A. Sarkar, J. Abell, P. Paturi, and H. Huhtinen, "Critical current density and pinning potential in $YBa_2Cu_3O_{7-\delta}$ thick films ablated from a $BaZrO_3$-doped nanocrystalline target," Supercond. Sci. Technol. **22**(4), 045014 (2009).
[52]T. Horide, S. Nagao, R. Izutsu, M. Ishimaru, R. Kita, and K. Matsumoto, "Geometric and compositional factors on critical current density in $YBa_2Cu_3O_{7-\delta}$ films containing nanorods," Supercond. Sci. Technol. **31**(6), 065012 (2018).
[53]S. R. Foltyn, L. Civale, J. L. Macmanus-Driscoll, Q. X. Jia, B. Maiorov, H. Wang, and M. Maley, "Materials science challenges for high-temperature superconducting wire," Nat. Mater. **6**(9), 631–642 (2007).
[54]X. Wang, F. J. Baca, R. L. Emergo, J. Z. Wu, T. J. Haugan, and P. N. Barnes, "Eliminating thickness dependence of critical current density in $YBa_2Cu_3O_{7-x}$ films with aligned $BaZrO_3$ nanorods," J. Appl. Phys. **108**(11), 113911 (2010).
[55]X. Wang, A. Dibos, and J. Z. Wu, "Weakening thickness dependence of critical current density in $YBa_2Cu_3O_{7-x}$ films using nanotube pore insertion," Phys. Rev. B **77**(14), 5 (2008).
[56]B. Villarejo, F. Pino, C. Pop, S. Ricart, F. Vallès, B. Mundet, A. Palau, P. Roura-Grabulosa, J. Farjas, N. Chamorro, R. Yáñez, X. Granados, T. Puig, and X.Obradors, "High performance of superconducting $YBa_2Cu_3O_7$ thick films prepared by single-deposition inkjet printing," ACS Appl. Electron. Mater. **3**(9), 3948–3961 (2021).
[57]X. Obradors, T. Puig, Z. Li, C. Pop, B. Mundet, N. Chamorro, F. Vallés, M. Coll, S. Ricart, B. Vallejo, F. Pino, A. Palau, J. Gázquez, J. Ros, and A. Usoskin, "Epitaxial $YBa_2Cu_3O_{7-x}$ nanocomposite films and coated conductors from $BaMO_3$ (M = Zr, Hf) colloidal solutions," Supercond. Sci. Technol. **31**(4), 044001 (2018).